16 Diffusion Tensor MRI Visualization

Q1

16.1 Introduction

Diffusion Tensor Magnetic Resonance Imaging (DT-MRI or DTI) is emerging as an important technology for elucidating the internal structure of the brain and for diagnosing conditions affecting the integrity of nervous tissue. DTI measurements of the brain exploit the fact that the network of fibers has a characteristic microstructure that constrains the diffusion of water molecules. The direction of fastest diffusion is aligned with fiber orientation in a pattern that can be numerically modeled by a *diffusion tensor*. DTI is the only modality for noninvasively measuring diffusion tensors in living tissue, making it especially useful for studying the directional qualities of brain tissue. Application areas include neurophysiology, neuroanatomy, and neurosurgery, as well as the diagnosis of edema (swelling), ischemia (brain damage from restricted blood flow), and certain types of brain tumors.

One of the fundamental problems in understanding and working with diffusion tensor data is its 3D and multivariate nature. Each sample point in a DTI scan can be represented by six interrelated values, and many features of interest are described in terms of derived scalar and vector fields, which are logically overlayed on the original tensor field. Thus, the central tasks of DTI visualization include the following:

1. Determining which aspects of the tensor field will be graphically conveyed,
2. Determining where that information must be displayed and where it can be ignored,
3. Visually abstracting the DTI quantities into the computer-graphics primitives with which the visualization is ultimately expressed.

This chapter gives background on the acquisition and mathematics of diffusion tensor imaging, and then surveys the current vocabulary of visualization methods used with DTI. We finish with some open questions that remain in the area of diffusion tensor visualization.

16.2 Diffusion Tensor Imaging

Appreciating the origin and physical significance of acquired scientific data is the first step in a principled approach to its visualization. This section briefly reviews the physical and mathematical underpinnings of diffusion tensor imaging.

Scientific understanding of the physical basis of diffusion converged at the beginning of the nineteenth century. In 1827, Robert Brown discovered the Brownian motion, which underlies the thermodynamic model of diffusion. He observed that pollen grains suspended in water exhibit a zigzag "random walk." This motion was hypothesized by Desaulx in 1877 to be the result of thermally energetic water molecules repeatedly colliding with the pollen grain. Einstein confirmed this hypothesis in 1905 as part of the development of his mathematical model of diffusion as a dynamically expanding Gaussian distribution [14]. The path of the pollen grain suspended in water is just a visible indicator of the similar Brownian motion of all liquid

molecules, whether in pure water, a porous medium, or biological tissue.

Many materials have intrinsic structural properties that constrain diffusion so that diffusivity is greater in some directions than in others; this is called *anisotropy*. If there is no directional variation in diffusion rates, the diffusion is called *isotropic*. Biological tissues often appear anisotropic because cell membranes and large protein molecules limit the motion of water molecules; this is termed *restricted diffusion* by Cooper *et al*.[8]. Dissections and histological studies have taught us that the grey matter of the brain is largely isotropic at the scale of MR scans, while the brain's white matter is more anisotropic, arising from the alignment of myelinated neuronal axons, which preferentially constrain water diffusion along the axon direction. Thus, via the mechanism of diffusion, the physical microstructure of white-matter tissue enables imaging of the neural pathways that connect the brain. DTI imaging measurements have been validated within acceptable error on the fibrous muscle tissue of the heart [31,16].

The measurement of diffusion in biological tissue is achieved with magnetic resonance imaging (MRI). In 1946, Purcell [29] and Block [6] independently discovered the nuclear magnetic resonance (NMR) effect. Water molecules contain hydrogen nuclei with uncoupled spins. In a strong magnetic field, the uncoupled spins cause the nuclei to align with and precess around the magnetic field direction, generating, in turn, a weak magnetic field aligned with the stronger ambient magnetic field. A second outside magnetic field can perturb this weak magnetic field; the magnetic resonance signal is the result.

In 1950, Erwin Hahn discovered an important NMR signal called the spin echo [15], and noted that the spin echo signal was perturbed by the diffusion of water molecules. Diffusion MR takes advantage of this effect and can thus measure hydrogen self-diffusivity in vivo. It is generally believed that the quantities we measure with diffusion MR are a mixture of intracellular diffusion, intercellular diffusion, and the exchange between the two sides of the cell membrane [34,32,33].

In 1973, Lauterbur described the principles of NMR imaging [20]. He encoded positioning information on NMR signals using gradient magnetic fields and the imaging-reconstruction algorithm. As a result, NMR imaging pinpoints the location where the signal is generated. This invention led to a new medical diagnostic instrument. In 1985, Bushel and Taylor combined the diffusion NMR and MR imaging techniques to create diffusion-weighted imaging [35]. A diffusion-weighted image (DWI) is a scalar-valued image that usually captures diffusion rate information in one direction. In a DWI, the effect of diffusion on an MRI signal is an attenuation; the measured image intensity can be related to the diffusion coefficient by the following equation [21]:

$$\tilde{I}(x, y) = I_0(x, y) \exp(\mathrm{bD}) \tag{16.1}$$

where $I_o(x, y)$ represents the voxel intensity in the absence of diffusion weighting, b characterizes the diffusion-encoding gradient pulses (timing, amplitude, shape) used in the MRI sequence, and D is the scalar diffusion coefficient.

Anisotropic diffusion information cannot be effectively represented in a scalar-valued DWI. In 1992, Basser et al. described the estimation of the diffusion tensor from the NMR spin echo [3]. The diffusion tensor, **D**, captures directional variation in the diffusion rate.

D is a 3×3 positive symmetric matrix:

$$\mathbf{D} = \begin{pmatrix} D_{xx} & D_{xy} & D_{xz} \\ D_{yx} & D_{yy} & D_{yz} \\ D_{zx} & D_{zy} & D_{zz} \end{pmatrix} \tag{16.2}$$

b is also now a 3×3 matrix, and it represents the diffusion encoding. The equation becomes

$$\tilde{I}(x, y) = I_0(x, y) \exp\left(- \sum_{i=1}^{3} \sum_{j=1}^{3} b_{ij} D_{ij} \right) \tag{16.3}$$

A diffusion tensor has three real eigenvalues, λ_1, λ_2, and λ_3. Each has a corresponding eigenvector, $\mathrm{v}_1, \mathrm{v}_2$, or v_3. A diffusion tensor is geometrically equivalent to an ellipsoid, and the

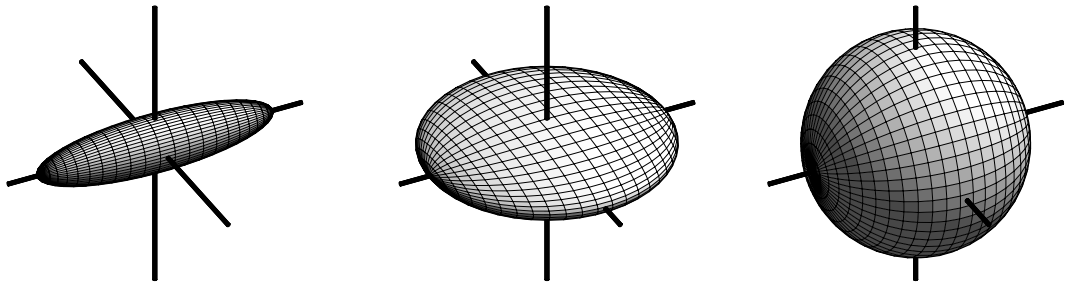

Figure 16.1 Ellipsoids represent diffusion tensors according the the eigensystem of the tensor: the eigenvalues are the radii of the ellipsoid, while the eigenvectors determine the orientations of the axes.

three eigenvectors of the diffusion-tensor matrix are set as the radii of the ellipsoid. The ellipsoid will match the shape that water diffuses to from the data point in a fixed amount of time. The ellipsoids in Fig. 16.1 depict the three types of spatial diffusion.

In regions of complex-diffusion anisotropy, such as the area where two fiber bundles cross or touch each other, a tensor does not accurately model the diffusion process. These areas of ambiguity can be addressed with a diffusion model that has more degrees of freedom than a second-order tensor. Tuch et al. acquire diffusion information in hundreds of directions to better resolve ambiguity [12,13].

16.3 Approaches for Visualizing DTI Datasets

16.3.1 Overview

DTI visualization is challenging because the data has high information content. A tensor field contains 3D patterns of matrix values, and there is no single well established method of displaying such information. Another challenge for DTI visualization methods is keeping the results properly grounded in the specific application domain for which the data was originally acquired. Without such a grounding, a visualization is unlikely to provide answers or generate new hypotheses about scientific problems.

Many DTI visualization approaches use a combination of scalar, vector, and tensor methods, contracting the tensor to appropriate scalars or vectors for a particular application. These derived fields can be used in many ways in visualization applications, and we will show a number of examples. In some cases, they are sufficient alone. From a practical standpoint, the use of derived fields is also an important strategy in keeping the information in the visualization to its essential minimum. Much of 3D DTI visualization struggles with precisely this issue—that is, which regions in the tensor field should contribute to the final visualization. The design of a visualization method is often a compromise between being informative and being legible. Part of what makes DTI visualization an exciting research topic is that the rules and strategies governing this design process are still being discovered.

16.3.2 Scalar Metrics

A common visualization approach involves contracting each tensor in a DTI to a scalar, reducing a DTI dataset to a scalar dataset. A carefully designed scalar metric can extract useful information while reducing the effect of noise. Some scalar metrics are rotationally invariant, which means that they do not depend on the coordinate system in which the tensor was measured. This tends to be a useful quality;

without it, knowledge of the coordinate system must always be carried along with the metric for proper interpretation.

The trace of the diffusion tensor $T_r(D) = D_{11} + D_{22} + D_{33}$ measures the mean diffusivity; it is rotationally invariant. It is demonstrated that, after induction of stroke, images representing the trace of the diffusion tensor provide a much more accurate delineation of the affected area than images representing the diffusion in only one direction [36].

Many of the scalar metrics derived from DTI measure the anisotropy of diffusion in different ways. Douek et al. defined an anisotropic diffusion ratio (ADR) $ADR_{xz} = \frac{D_{xx}}{D_{zz}}$ for the anisotropy index [10]. Gelderen et al. calculated a measure of diffusion anisotropy as the standard deviation of the three diffusion coefficients $A = \sqrt{\frac{1}{6}} \frac{\sqrt{(D_{xx}-D_{av})^2 + (D_{yy}-D_{av})^2 + (D_{zz}-D_{av})^2}}{D_{av}}$ to study the stroke [36]. Both of these metrics are rotationally variant.

Basser et al. have calculated rotationally invariant anisotropy metrics from the diffusion tensor [4]: relative anisotropy

$$RA = \frac{\sqrt{(\lambda_1 - <\lambda>)^2} + \sqrt{(\lambda_2 - <\lambda>)^2} + \sqrt{(\lambda_3 - <\lambda>)^2}}{\sqrt{3 <\lambda>}} \tag{16.4}$$

and fractional anisotropy

$$FA = \sqrt{\frac{3}{2}} \frac{\sqrt{(\lambda_1 - <\lambda>)^2} + \sqrt{(\lambda_2 - <\lambda>)^2} + \sqrt{(\lambda_3 - <\lambda>)^2}}{\sqrt{\lambda_1^2 + \lambda_2^2 + \lambda_3^2}} \tag{16.5}$$

where $<\lambda> = \frac{\lambda_1+\lambda_2+\lambda_3}{3}$

Pierpaoli et al. compared the two kinds of metrics and showed that rotationally invariant metrics consistently show a higher degree of anisotropy than their variant analogs [27]. But because *RA* and *FA* are calculated over one diffusion tensor, they are still susceptible to noise contamination. Pierpaoli et al. calculated an inter-voxel anisotropy index, the *lattice index (LI)*, which locally averages inner products between diffusion tensors in neighboring voxels. *LI* has a low error variance and is less susceptible to bias than are other rotationally invariant metrics.

Scalar anisotropy metrics such as *FA* and *RA* convey how anisotropic a diffusion distribution may be, but they do not convey whether the anisotropy is linear, planar, or some combination of the two. In terms of ellipsoid glyphs, cigar-shaped and pancake-shaped ellipsoids can have equal *FA* although their shapes differ greatly. Westin et al. [39] more completely model diffusion anisotropy with a set of three metrics that measure linear, planar, and spherical diffusion: $c_l = \frac{\lambda_1-\lambda_2}{\lambda_1}$, $c_p = \frac{\lambda_2-\lambda_3}{\lambda_1}$, and $c_s = \frac{\lambda_3}{\lambda_1}$, respectively. By construction, $c_l + c_p + c_s = 1$. Thus, these three metrics parameterize a barycentric space in which the three shape extremes (linear, planar, and spherical) are at the corners of a triangle, as shown in Fig. 16.2.

One way to qualitatively compare some of the metrics described above is shown in Fig. 16.3, where we sample their values on a slice of DTI data from a brain. Notice that the trace (*Tr*) is effective at distinguishing between the cerebral–spinal fluid (where *Tr* is high) and the brain tissue (lower *Tr*), but it fails to differentiate between different kinds of brain tissue. High fractional anisotropy *FA*, on the other hand, indicates white matter, because the directional structure of the axon bundles permits faster diffusion along the neuron fiber direction than across it. *FA* is highest inside thick regions of uniformly anisotropic diffusion, such as inside the corpus callosum, the bridge between the two hemispheres of the brain. Finally, while both c_l and c_p indicate high anisotropy, their relative values indicate the shape of the anisotropy.

16.3.3 Eigenvector Color Maps

When diffusion tensors are measured with MRI, each tensor is represented by a 3×3 symmetric matrix; the values in the matrix are measured relative to the coordinate frame of the MRI scanner. Because they are real-valued,

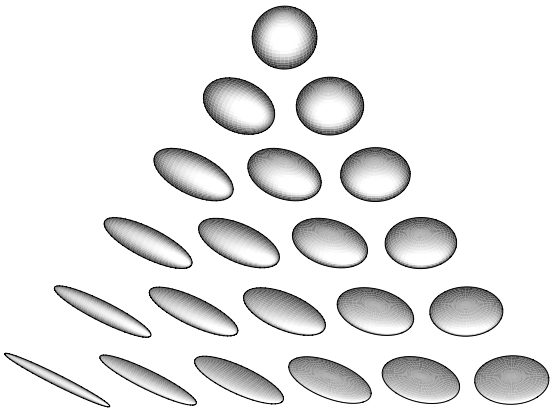

Figure 16.2 Barycentric space of diffusion tensor shapes

diffusion tensors have three real eigenvalues and three orthogonal eigenvectors. The eigenvalues are all nonnegative, because negative diffusivity is physically impossible. The eigenvectors define the orientation of the diffusion tensor. The *major* or *principal* eigenvector is associated with the largest eigenvalue and defines the direction of fastest diffusion. This direction can have significant physical meaning. In DTI scans of nervous tissue, the principal eigenvector is aligned with the coherent fibers.

A common visualization goal is to depict the spatial patterns of the principal eigenvector only in regions where it is meaningful, rather than give a complete depiction of all the tensor information. Visualizing these patterns is often an important step in verifying that a given DTI scan has succeeded in resolving a feature of interest. A simple spherical color map of the principal eigenvector is the standard tool for this task, which first assigns an (R,G,B) color according to the (X,Y,Z) components of the principal eigenvector, v_1,

$$R = \mathrm{abs}(\mathrm{v}_{1x}), \quad \mathrm{G} = \mathrm{abs}(\mathrm{v}_{1y}), \quad \mathrm{B} = \mathrm{abs}(\mathrm{v}_{1z}),$$

and then modulates the saturation of the RGB color with an anisotropy metric. The direction of the principal eigenvector is numerically ill-defined when the tensor is isotropic, or has mostly planar anisotropy, in which case the visualization should not imply a particular direction with the hue of the RGB color. Thus, the saturation is modulated by c_l. Also, note that by design, the same color is assigned to v and $-$v. This also has a mathematical justification. The sign of eigenvectors is not defined. Numerical routines for their calculation may return either of two opposing vectors,

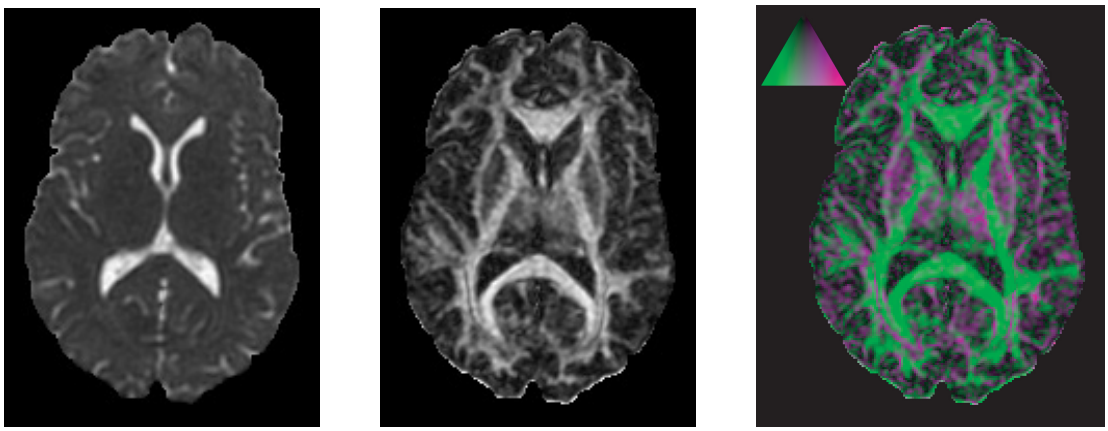

(a) *Tr*: Trace (b) *FA*: fractional anisotrophy (c) C_L(green) and C_P (magenta)

Figure 16.3 Different shape metrics applied to one slice of a brain DTI scan

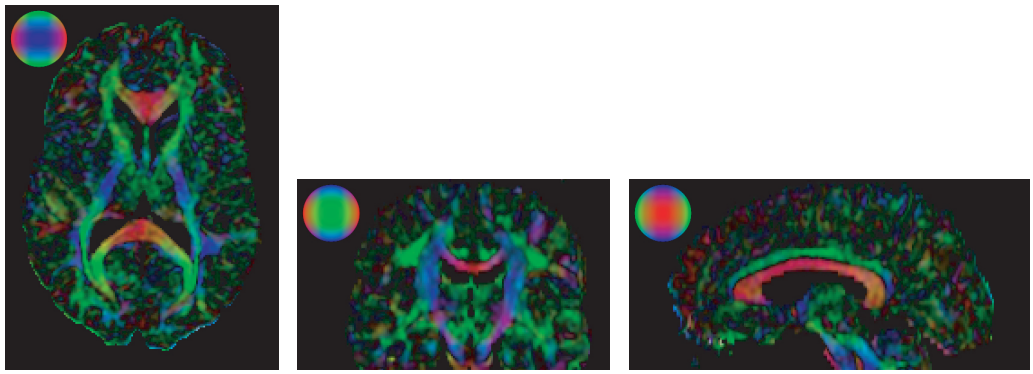

Figure 16.4 Eigenvector color maps shown on axis-aligned slices, with three different slice orientations. The two axes within the slice are given with the anatomical name of the slice orientation.

both of which should be visualized identically. Fig. 16.4 shows three examples of the the eigenvector color map applied to the principal eigenvector.

16.3.4 Glyphs

A glyph is a parameterized icon that represents the data with its shape, color, texture, location, etc. Over the years, researchers have come up with multiple glyphs suitable for DTI visualization. We review and compare some of them here.

Diffusion ellipsoids are surfaces of constant mean-squared displacement of diffusing water molecules at some time τ after they are released at the center of each voxel. Ellipsoids are a natural choice of glyph to summarize the information contained in a diffusion tensor [27]. The three principle radii are proportional to the eigenvalues and the axes of the ellipsoid aligned with the three orthogonal eigenvectors of the diffusion tensor. The size of an ellipsoid can be associated with the mean diffusivity. The preferred direction of diffusion is indicated by the orientation of the diffusion ellipsoid. Arrays of ellipsoids can be arranged together in the same order as the data points to show a 2D slice of DTI data. Laidlaw et al. normalized the size of the ellipsoids to fit more of them in a single image [19] (Fig. 16.5). While this method loses the ability to show mean diffusivity, it creates more uniform glyphs that better show anatomy and pathology over regions.

They also described a method that uses the concepts of brush strokes and layering from oil painting. They used 2D brush strokes both individually, to encode specific values, and collectively, to show spatial connections and to generate texture and a sense of speed corresponding to the speed of diffusion. Layering and contrast were used to create depth. The

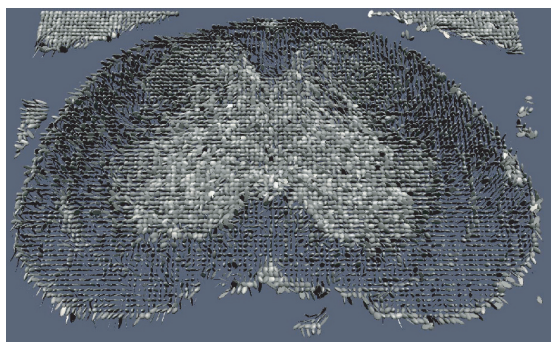

Figure 16.5 Arrays of normalized ellipsoids visualize the diffusion tensors in a single slice

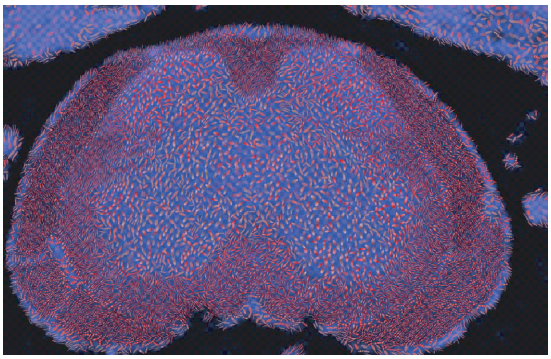

Figure 16.6 Brush strokes illustrate the direction and magnitude of the diffusion: background color and texture map show additional information

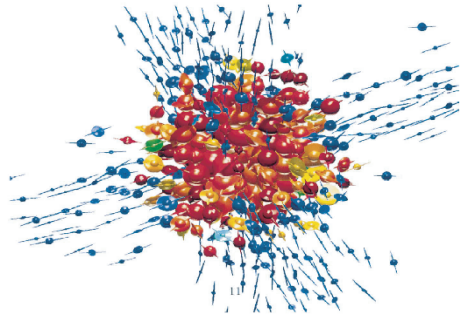

Figure 16.7 The composite shape of linear, planar, and spherical components emphasizes the shape of the diffusion tensor.

method was applied to sections of spinal cords of mice with Experimental Allergic Encephalomyelitis (EAE) and clearly showed anatomy and pathology (Fig. 16.6).

In a still image it is often hard to tell the shape of an ellipsoid with only surface shading information. Westin et al. used a composite shape of linear, planar, and spherical components to emphasize the shape of the diffusion ellipsoids [38]. The components are scaled to the eigenvalues, but can alternatively be scaled according to the shape measures c_l, c_p and c_s. Additionally, the color of the glyph is interpolated between the blue linear case, yellow planar case, and red spherical case (Fig. 16.7).

Kindlmann's approach adapted superquadrics, a traditional surface-modeling technique [1], as tensor glyphs. He created a class of shapes that includes spheres in the isotropic case, while emphasizing the differences among the eigenvalues in the anisotropic cases. As demonstrated in Fig. 16.8, cylinders are used for linear and planar anisotropy, while intermediate forms of anisotropy are represented by approximations to boxes. As with ellipsoid glyphs, a circular cross-section accompanies equal eigenvalues for which distinct eigenvectors are not defined.

The differences among the glyph methods can be appreciated by comparison of their results on a portion of a slice of a DTI brain scan, as

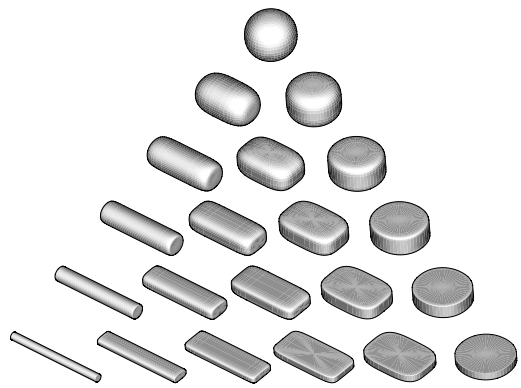

Figure 16.8 Superquadrics as tensor glyphs, sampling the same barycentric space as in Fig. 16.2

shown in Fig. 16.9. The individual glyphs have been colored with the principal eigenvector color map. The directional cue given by the edges of box glyphs is effective in linearly anisotropic regions, but it can be misleading in regions of planar anisotropy and isotropy, since in these cases the corresponding eigenvectors are not numerically well defined. The rotational symmetry of ellipsoid glyphs avoids misleading depictions of orientation, with the drawback that different shapes can be hard to distinguish. The superquadric glyphs aim to combine the best of the box and ellipsoid methods.

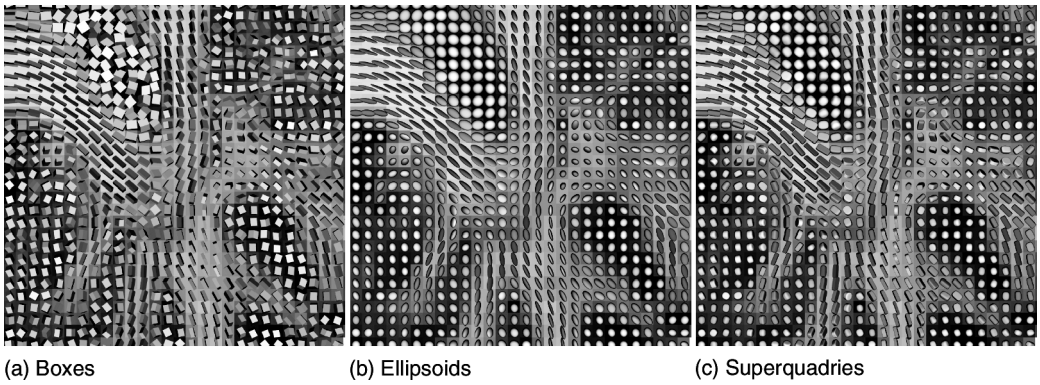

Figure 16.9 A portion of a brain DTI scan (also used in Figs. 16.3 and 16.4) as visualized by three different glyph methods. The overall glyph sizes have been normalized.

16.3.5 Tractography

In glyph-based methods, each glyph represents one diffusion tensor. Tractography, a term first applied to DTI analysis by Basser [2], yields curves of neural pathways, which are continuous and hard to represent using discrete glyphs. Streamlines and their derivatives are widely used for tractography results. Xue et al. show the result of fiber projection reconstruction by hand-selecting seeding points in a ROI and displaying the curves generated from them [40]. The colors represent different groups of fiber structures. Zhang et al. used streamtubes and streamsurfaces to visualize the diffusion tensor field [41]. Streamtubes visualize fiber pathways tracked in regions of linear anisotropy: the trajectories of the streamtubes follow the major eigen vectors in the diffusion tensor field; the color along the streamtubes represents the magnitude of the linear anisotropy; the cross-section shape represents the medium and minor eigenvectors. Streamsurfaces visualize regions of planar anisotropy: the streamsurface follows the expansion of major and medium eigenvectors in the diffusion tensor field, and the color is mapped to the magnitude of planar anisotropy.

Zhang et al. used a culling algorithm to control the density of the streamtubes in the scene [41] so that inside structures are visible and outside structures are still adequately represented. The metrics for the culling process include the length of a trajectory, the average linear anisotropy along a trajectory, and the similarity between a trajectory and the group of trajectories already selected.

A significant problem with trajectories calculated by integration happens in regions where the white-matter structures change quickly. Pierpaoli et al. showed that incorrect spurious connections can easily be generated [26]. Each diffusion tensor measurement is made over a small region. If the tissue is coherent in direction structure throughout that region, then the measurement will be consistent. Otherwise, the tensor will be an amalgam of all the different values in the small region, and the major eigenvector may not point along a tract. These problems happen where tracts cross, diverge, or are adjacent to other tissues. Tractography is also sensitive to noise; a small amount of noise can cause significantly different results.

Some researchers have tried to address these problems by regularizing diffusion datasets [5,42,37] or direction maps [28,23]. Some researchers have explored new ways to find connectivity. Brun et al. use sequential importance sampling to generate a set of curves, labeled with probabilities, from each seed point [7].

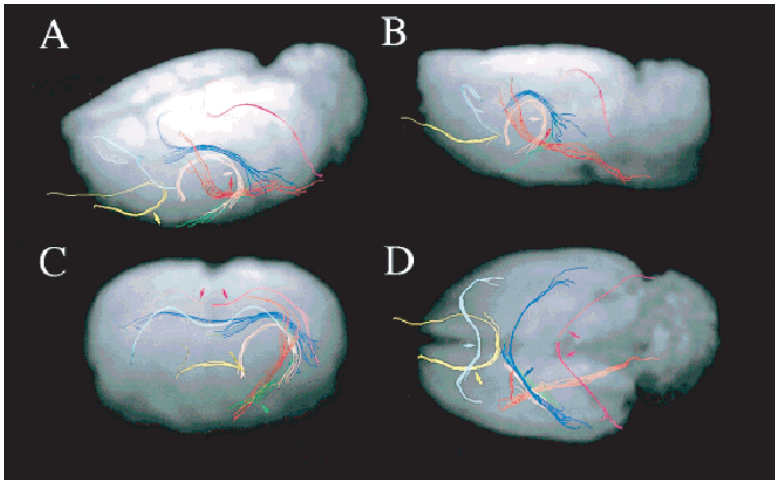

Figure 16.10 Xue et al. show the result of tractography with streamlines.

Batcherlor et al. generate an isosurface of solution by solving a diffusion-convection equation [25]. Parker et al.use front propagation in fast-marching tractography [24]. High angular resolution diffusion imaging is reported to ameliorate ambiguities in regions of complex anisotropy [12,13] and may ultimately be the best solution to this problem.

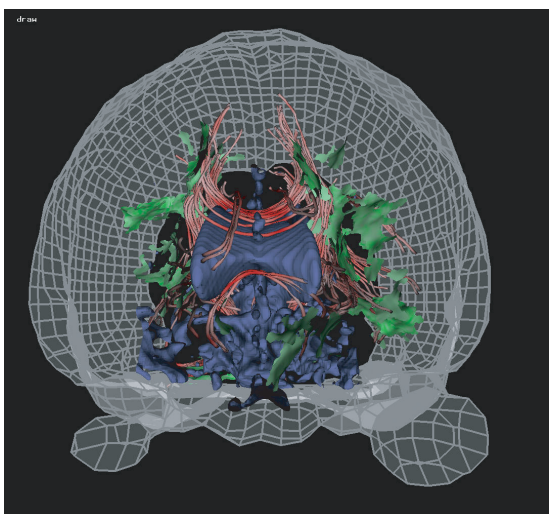

Figure 16.11 Red streamtubes and green streamsurfaces show linear and planar anisotropy, respectively, together with anatomical landmarks for context.

16.3.6 Volume-Rendering

Glyphs and tractography communicate field structure with discrete geometry: the poly-line or cylinder represents a fiber tract or the faceted surface of an polygonal ellipsoid, for example. Direct volume-rendering, on the other hand, sidesteps the creation of intermediate geometry, and maps ''directly'' from measured properties of the field to optical properties like color and opacity, which are then composited and shaded [22,11]. The mapping is performed by the transfer function, which must be carefully designed to emphasize and delineate the features of interest, while not obscuring them with unimportant regions. In direct volume-rendering of scalar data, the transfer function often maps from the scalar data values to opacity, although greater specificity and expressivity are possible with higher-dimensional and multivariate transfer functions [18]. Because transfer functions are applied without respect to position in the field, direct volume-rendering has the potential to effectively convey large-scale patterns across the entire dataset.

Kindlmann et al. have explored various types of diffusion tensor transfer functions [17]; the present discussion will focus on transfer functions of tensor shape because of their intuitive definition and useful results.

The barycentric space of tensor shapes shown in Figs. 16.2 and 16.8 captures two important degrees of freedom (from the total six) in a tensor field: degree and type of anisotropy. This space does not represent changes in overall size or changes in orientation, but these are not crucial for visualizing the structure of white-matter fiber tracts. Fig. 16.3a indicated that the trace, *Tr*, does not vary significantly between gray and white matter, and typically, the structural organization that distinguishes white matter is interesting irrespective of its orientation.

Fig. 16.13 demonstrates the results of using the barycentric shape space as the domain of transfer functions that assign opacity only.

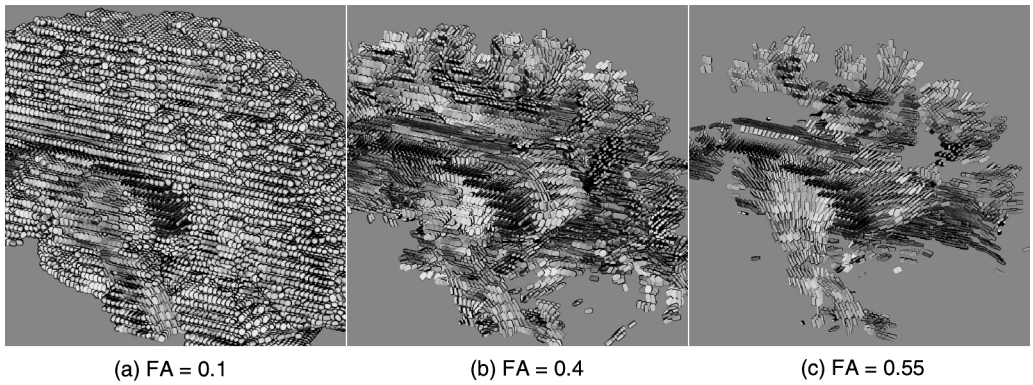

Figure 16.12 Glyph-based visualization of a volumetric portion of a brain DTI scan (also used in Figs. 16.3, 16.4, and 16.9), with glyph culling based on three different fractional anisotropy thresholds.

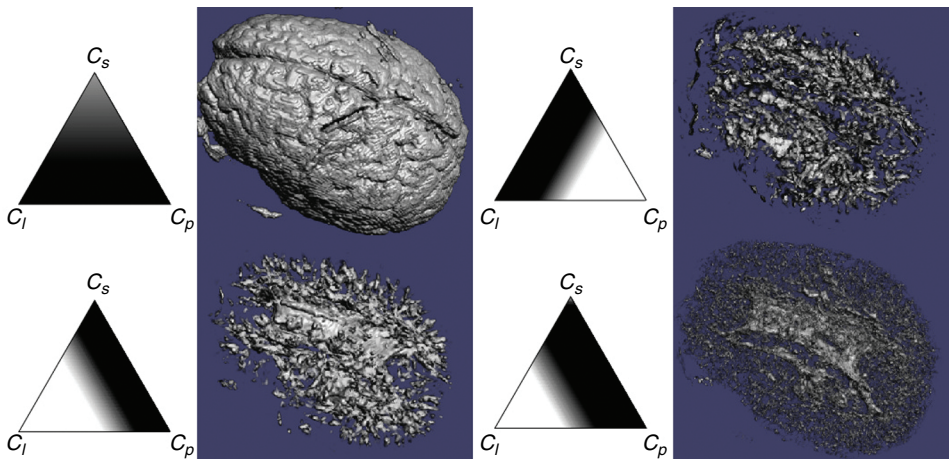

Figure 16.13 Four different barycentric opacity maps and the corresponding renderings

These renderings were produced with a brute-force renderer that samples each image ray at multiple points within the field, interpolates the tensor field component-wise, calculates the eigenvalues and the shape metrics (c_l, c_p, c_s), and then looks up the opacity for that sample. In the left side of Fig. 16.13, the overall shape of the brain is seen when opacity is assigned to high c_s (isotropic) samples, while the shape of the white matter is visible when opacity assignment is limited to high c_l values. Arbitrary combinations of shape may be emphasized with this sort of transfer function (Fig. 16.13, right). Fig. 16.14 shows how specifying color as a function of barycentric shape can create a more informative rendering: the color variations indicate which portions of the field are more or less planarly anisotropic.

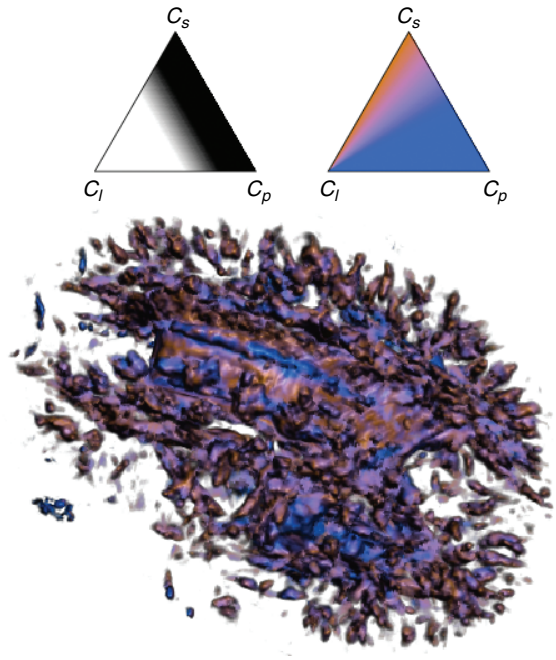

Figure 16.14 Assigning color and opacity with barycentric transfer function

16.4 Open Issues

Interest and activity in diffusion tensor visualization have been steadily increasing with the expanding applications of tensor imaging, increased computation and graphics capabilities for display, and advances in the visualization methods themselves. There are several important open issues and design challenges that merit consideration and further research.

Visual design of glyphs: Glyphs must be parameterizable by at least as many variables as we intend to display through them. On the other hand, they should also be concise and compact, so that multiple glyphs viewed next to, or on top of, each other can still usefully convey information. This is a daunting task for depicting complex 3D patterns in the tensor field. Inspiration may be drawn from different artistic traditions of painting and technical illustration.

Seeding and culling schemes: While it is easy to survey information everywhere over a 2D domain, this is impossible in three dimensions because of occlusion. The task of glyph placement, trajectory placement, or selection of any visual abstraction is a difficult problem of visual optimization; the result must be legible in multiple contradictory ways. The interconnected nature of the white-matter fiber tracks in the brain does not make this task easy. Solving this optimization may involve level-of-detail information and user-defined regions of interest.

Computational validation: This is perhaps the hardest part of doing scientifically *useful* visualization. An unresolved issue in DTI visualization is the extent to which the paths calculated by fiber tracking correspond to the paths of actual axons in the white matter. Locally, the fiber direction does correspond to tissue organization, and the major "trunk lines" of connectivity are known from neuroanatomy. However, tractography methods can produce long and circuitous paths of purported connectivity whose actual validity is not, and can not easily be, known. Scanning diffusion phantoms (with known connectivity) might address this, as would advances in histological preparations.

Display devices and interaction: DTI datasets are complicated and inherently 3D. Many visualizations involve large, complex graphical models. Recent advances in display may help boost the capabilities and applications of the visualization. Especially promising is the use of immersive virtual reality for displaying complex 3D fields of neural structures. But questions remain about the relative value of different display and interaction environments.

Visual validation: No one visualization method stands out as the ''gold standard'' by which others are judged. Every method has advantages and limitations based on what types of information it seeks to convey and the specific techniques that are used to convey it. Currently, most visualization methods are judged by their own inventors. User studies and other validation methods will both help justify the methods in a more objective way and help evaluate different interaction environments.

Modeling: The interaction between water molecules and biological structures is vital for understanding the information contained in diffusion tensor images. It is generally believed that the sheath outside the neural axons causes most of the restrictions on water diffusion. Less is known about locations where fiber bundles diverge, cross, or kiss. What is the contribution of intracellular diffusion, intercellular diffusion, and exchange between the membranes? A physically realistic model may help us analyze the tensor data and then visualize the underlying structures in a meaningful way.

16.5 Summary

Since DTI technology emerged 10 years ago, DTI acquisition, visualization, analysis, and application have spurred numerous multidisciplinary efforts. For scientific visualization students, the problem is especially intriguing, because DTIs are large 3D multivariate datasets; they present many challenges for visualization. On the other hand, the problem has real-world origins and applications, and many challenges: The datasets are noisy, resolution is never sufficient, and partial volume effects limit the results. Perhaps the greatest challenge is the breadth of knowledge necessary to truly understand the entire process, from patient to imaging to computation to visual analysis back to patient.

In this chapter, we have given a brief survey of the last 10 years of visualization-related research, including some of the issues that remain to resolve. We look forward to the next 10 years, during which we expect that much more of the tremendous potential of this imaging modality will be realized.

References

1. A. Barr. Superquadrics and angle-preserving transformations. *IEEE Computer Graphics and Applications*, 18(1):11–23, 1981.
2. P. J. Basser, S. Pajevic, C. Pierpaoli, J. Duda, and A. Aldroubi. *In vivo* fiber tractography using DT-MRI data. *Magnetic Resonance in Medicine*, 44:625–632, 2000.
3. P. J. Basser, J. Mattiello, and D. LeBihan. Estimation of the effective self-diffusion tensor from the NMR spin echo. *J Magn Reson B.*, 103(3):247–54, March 1994.
4. P. J. Basser and C. Pierpaoli. Microstructural features measured using diffusion tensor imaging. *Journal of Magnetic Resonance, Series B*, pages 209–219, 1996.
5. M. Bjornemo, A. Brun, R. Kikinis, and C.-F. Westin. Regularized stochastic white matter tractography using diffusion tensor MRI. In *MICCAI2002*, 2002.
6. F. Bloc. Nuclear induction. *Physical Review*, 70:460–474, 1946.
7. A. Brun, M. Bjornemo, R. Kikinis, and C.-F. Westin. White matter tractography using sequential importance sampling. In *ISMRM 2002*, 2002.
8. R. L. Cooper, D. B. Chang, A. C. Young, C. J. Martin, and B. Ancker-Johnson. Restricted diffusion in biophysical systems. *Biophysical Journal*, 14:161–177, 1974.
9. T. Delmarcelle and L. Hesselink. Visualizing second-order tensor fields with hyperstream lines. *IEEE Computer Graphics and Applications*, 13(4):25–33, 1993.
10. P. Douek, R. Turner, J. Pekar, N. Patronas, and D. LeBihan. MR color mapping of myelin fiber orientation. *J. Comput. Assist. Tomogr*, 15:923–929, 1991.

11. R. A. Drebin, L. Carpenter, and P. Hanrahan. Volume rendering. *Computer Graphics*, 22(4): 65–74, 1988.
12. D. S. Tuch, R. M. Weisskoff, J. W. Bellireau, and V. J. Wedeen. High angular resolution diffusion imaging of the human brain. In *Proceedings of the 7th Annual Meeting of ISMRM*, page 321, 1999.
13. D. S. Tuch, R. M. Weisskoff, J. W. Bellireau, and V. J. Wedeen. High angular resolution diffusion imaging reveals intravoxel white matter fiber heterogeneity. *Magn. Reson. Med.*, 48(4):577–582, October 2002.
14. A. Einstein. Über die von der molekularkinetischen Theorie der Wärme geforderte bewegung von in ruhenden Flüssigkeiten suspendierten teilchen. *Annalen der Physik*, 17:549–560, 1905.
15. E. L. Hahn. Spin echoes. *Physical Review*, 80:580–594, 1950.
16. E. W. Hsu, A. L. Muzikant, S. A. Matulevicius, R. C. Penland, and C. S. Henriquez. Magnetic resonance myocardial fiber-orientation mapping with direct histological correlation. *Am J Physiol*, 274:H1627–1634, 1998.
17. G. Kindlmann, D. Weinstein, and D. A. Hart. Strategies for direct volume rendering of diffusion tensor fields. *IEEE Transactions on Visualization and Computer Graphics*, 6(2):124–138, 2000.
18. J. Kniss, G. Kindlmann, and C. Hansen. Multidimensional transfer functions for interactive volume rendering. *IEEE Transactions on Visualization and Computer Graphics*, 8(3):270–285, 2002.
19. D. H. Laidlaw, E. T. Ahrens, D. Kremers, M. J. Avalos, C. Readhead, and R. E. Jacobs. Visualizing diffusion tensor images of the mouse spinal cord. In *Proceedings of IEEE Visualization 1998*, pages 127–134, October 1998.
20. P. C. Lauterbur. Image formation by induced local interactions: examples employing nuclear magnetic resonance. *Nature*, 242:190–191, 1973.
21. D. LeBihan. Molecular diffusion nuclear magnetic resonance imaging. *Magn. Reson. Quant*, 17:1–30, 1991.
22. M. Levoy. Display of Surfaces from Volume Data. *IEEE Computer Graphics & Applications*, 8(5):29–37, 1988.
23. O. Coulon, D. C. Alex er, and S. R. Arridge. Tensor field regularisation for DT-MR images. In *Proceedings of British Conference on Medical Image Understanding and Analysis*, 2002.
24. G. J. M. Parker, K. E. Stephen, G. J. Barker, J. B. Rowe, D. G. MacManus, C. A. M. Wheeler-Kingshott, O. Ciccarelli, R. E. Passingham, R. L. Spinks, R. N. Lemon, and R. Turner. Initial demonstration of *in vivo* tracing of axonal projections in the macaque brain and comparison with the human brain using diffusion tensor imaging and fast marching tractography. *NeuroImage*, 15:797–809, 2002.
25. P. G. Batchelor, D. L. G. Hill, D. Atkinson, F. Calamanten, and A. Connellyn. Fibre-tracking by solving the diffusion-convection equation. In *Proceedings of ISMRM 2002*, 2002.
26. C. Pierpaoli, A. S. Barnett, S. Pajevic, A. Virta, and P. J. Basser. Validation of DT-MRI tractography in the descending motor pathways of human subjects. In *International Society for Magnetic Resonance in Medicine (ISMRM)*, Glasgow, page 501, 2001.
27. C. Pierpaoli and P. J. Basser. Toward a quantitative assessment of diffusion anisotropy. *Magn Reson Med.*, 36(6):893–906, 1996.
28. C. Poupon, C. A. Clark, V. Frouin, J. Regis, I. Block, D. LeBihan, and J.-F. Mangin. Regularization of diffusion-based direction maps for the tracking of brain white matter fascicles. *NeuroImage*, 12:184–195, 2000.
29. E. M. Purcell, H. C. Torrey, and R. V. Pound. Resonance absorption by nuclear magnetic moments in a solid. *Physical Review*, 69, 1946.
30. R. R. Dickinson. A unified approach to the design of visualization software for the analysis of field problems. In *Three-dimensional Visualization and Display Technologies (Proceedings of SPIE)*, pages 173–180, 1989.
31. D. F. Scollan, A. Holmes, R. Winslow, and J. Forder. Histological validation of myocardial microstructure obtained from diffusion tensor magnetic resonance imaging. *Am J Physiol*, 275:2308–2318, 1998.
32. G. J. Stanisz, A. Szafer, G. A. Wright, and R. M. Henkelman. An analytical model of restricted diffusion in bovine optic nerve. *Magn Reson Med*, 37(1):103–11, 1997.
33. G. J. Stanisz and R. M. Henkelman. Tissue compartments, exchange and diffusion. In *Workshop on Diffusion MRI: Biophysical Issues*, pages 34–37, 2002.
34. A. Szafer, J. Zhong, and J. C. Gore. Theoretical model for water diffusion in tissues. *Magn Reson Med*, 33:697–712, 1995.
35. D. G. Taylor and M. C. Bushell. The spatial mapping of translational diffusion coefficients by the NMR imaging technique. *Physics in Medicine and Biology*, 30:345–349, 1985.
36. P. van Gelderen, M. H. de Vleeschouwer, D. DesPres, J. Pekar, P. C. van Zijl, and C. T. Moonen. Water diffusion and acute stroke. *Magn Reson Med*, 31:154–63, 1994.

Q5

Q6

Q7
37. D. M. Weinstein, G. L. Kindlmann, and E. C. Lundberg. Tensorlines: advection diffusion-based propagation through diffusion tensor fields. In *IEEE Visualization '99*, pages 249–254, 1999.
38. C.-F. Westin, S. E. Maier, H. Mamata, A. Nabavi, F. A. Jolesz, and R. Kikinis. Processing and visualization for diffusion tensor MRI. *Medical Image Analysis*, 6:93–108, 2002.
39. C. F. Westin, S. Peled, H. Gubjartsson, R. Kikinis, and F. A. Jolesz. Geometrical diffusion measures for MRI from tensor basis analysis. In *Proceedings of ISMRM*, April 1997.
Q8
40. R. Xue, Peter C. M, van Zijl, B. J. Crain, M. Solaiyappan, and S. Mori. In vivo three-dimensional reconstruction of rat brain axonal projections by diffusion tensor imaging. *Magnetic Resonance in Medicine*, 42:1123–1127, 1999.
41. S. Zhang, C. Demiralp, and D. H. Laidlaw. Visualizing diffusion tensor MR images using streamtubes and streamsurfaces. *IEEE Transactions on Visualization and Computer Graphics*, 2003.
42. L. Zhukov and A. Barr. Oriented tensor reconstruction: tracing neural pathways from diffusion tensor MRI. In *Proceedings of the conference on Visualization '02*, pages 387–394, 2002.
Q9

AUTHOR QUERIES

Q1 Au: author name?
Q2 Au: ok?
Q3 Au: Please review references for completeness and accuracy, see, e.g., 23?
Q4 Au: page numbers?
Q5 Au: ?
Q6 Au: pages?
Q7 Au: pages?
Q8 Au: pages?
Q9 Au: page/issue/volume info?